Proceedings of the 2nd EAA International
Symposium on Hydroacoustics
24-27 May 1999, Gdańsk-Jurata
POLAND

Pressure Field Produced by Some Finite Amplitude Sources

Grażyna Grelowska

Naval Academy, ul. Smidowicza 71, 81-919 Gdynia, POLAND
e-mail: grelowska@amw.gdynia.pl

Pressure field of finite amplitude sources is examined in the paper. Detailed measurements of nonlinear distortion within beams radiated by plane and focused circular pistons are presented. Comparison of experimental results are made with numerical calculations based on the nonlinear parabolic wave equation (KZK) with the equivalent boundary condition adequate to the actual boundary condition. Special attention is paid to impact that the pressure distribution at the radiating surface has on the phenomena occurring in the vicinity of the source. Focused beam is examined over a distance extending up to post focal region. Investigation is carried out with various pressure amplitude at the source in pseudo continuous wave conditions.

1. Introduction

Finite amplitude sources find miscellaneous ways of practical application in many areas, especially in medicine [9, 12, 15] and industry [10, 14, 18]. Both plane and focused sources are used widely in either continuous wave or pulsed mode, and at intensities which lead to non-linear effects such as harmonic generation and shock formation. Typical ultrasonic sources generate strong diffraction phenomena, which combine with finite amplitude effects to produce waveforms that vary from point to point within the sound beam.

In many applications the most important are phenomena occurring in the nearfield area. It is caused by the fact that due to the applied measurement set up arrangement and the chosen parameters of used transducers the measured or diagnosed object is often situated within the nearfield area.

Many papers have been published devoted to the problem of the nonlinear distortion of the finite amplitude wave in the nearfield of the source. The fine structure of the nearfield presents difficulties to both: the theoretical and the experimental investigations. One of the first papers devoted to the theoretical description of the nearfield of the finite amplitude source was published in 1971 by Ingenito and Williams Jr. [17]. There the second harmonic field of a piston transducer was calculated by means of the perturbation method. The pioneering investigations of nonlinear effects in directional sound beams were performed by Bakhvalov *et al.* [8]. A significant step was made by Norwegian scientist, who solved the KZK equation numerically, using the finite difference scheme [1], which is known as the Bergen code. It accounts for the nonlinearity, absorption and diffraction. The solution is widely used in comparing the measurement results [5, 24] and may be modified according to the measurements conditions. The algorithms used in the computation are permanently improved and developed, among them may be mentioned such as: the time domain algorithm based on the nonlinear progressive-wave equation (NPE) [23], the time-domain algorithm developed by Lee and Hamilton based on a modified form of the KZK equation [19] and the frequency-domain algorithm without restriction of the area of validity in the vicinity of the source elaborated by Filipczyński *et al.* [13].

Sources of different shape are used in investigations, for instance plane and focused circular sources [3] and rectangular sources [6, 20]. Underwater focused sources, reported in literature, could be divided into two groups. The first one consists of sources with additional lens [4, 21, 22] and the second one - of a single PZT element [2, 16]. In experiments performed by B.

G. Lucas, T. G. Muir the concentrating biconcave polystyrene lens was separated from radiating plane element, while A. C. Baker used plano-concave lenses coupled to the transducer face.

The purpose of the paper is to review measurements of finite amplitude sound beam in water, both focused and unfocused, and compare them with predictions obtained using a frequency domain algorithm for solving KZK equation. The conducted investigations enrich data concerning field of plane finite amplitude circular sources with uniform and nonuniform pressure distribution at the radiating surface. In the experiments are used also focused sources of two mentioned above types: the first - consisting of a single PZT bowl element and the second - manufactured in the form of plano-concave PMM lens joined with a PZT circular source. The purpose of the investigation is the observation of the pressure field distribution and growth of nonlinear distortion of finite amplitude wave within a beam and especially the changes in spatial distribution of fundamental and higher harmonic components.

2. Theory

The theoretical predictions are obtained from numerical solution of the KZK nonlinear parabolic wave equation, written in terms of sound pressure p:

$$\frac{\partial^2 p}{\partial z \partial \tau} = \frac{c_o}{2}\left(\frac{\partial^2}{\partial r^2} + \frac{1}{r}\frac{\partial p}{\partial r}\right) + \frac{b}{2\rho_o c_o^3}\frac{\partial^3 p}{\partial \tau^3} + \frac{\beta}{2\rho_o c_o^3}\frac{\partial^2 p^2}{\partial \tau^2} \quad (1)$$

Only axisymmetric radiation is considered, with z the coordinate along the axis of the sound beam, r the distance from the beam axis, and $\tau = t - z/c_o$ a retarded time, where c_o is the propagation speed. The first term on the right-hand side of Eq. (1) accounts for diffraction. Thermoviscous attenuation is taken into account by the second term, where b is the dissipation coefficient and ρ_o is the ambient density of the fluid. In the third term, $\beta = 1 + B/A$ denotes the coefficient of nonlinearity. In general Eq. (1) is an accurate model of the pressure field produced by directional sources ($ka >> 1$, where k characterises the wave number and a the radius of the source) at distances beyond a few source radii and in regions close to the source, the paraxial region (up to about 20° off the axis in the far field) The restriction is satisfied in most practical applications of directional sound beams. A complete discussion of the domain of validity of the KZK equation for plane and focused piston sources is provided in [26, 27].

The boundary condition for the plane circular source with uniform velocity amplitude and radius a are given in the following form:

$$p(\vec{r}, z=0, t) = p_o \sin(\omega_o t)\, H\left(\frac{|\vec{r}|}{a}\right) \quad (2)$$

where p_o is the effective pressure amplitude at the source, ω_o is the angular frequency, and H is the Heaviside unit step function. Since the order of accuracy of the KZK equation is consistent with the use of the linear plane wave impedance relation [25] $p = \rho_o c_o u$, where u is the particle velocity in the z direction, the boundary condition (2) can be expressed in terms of pressure rather than particle velocity. In all calculations and experiments $f_o = \omega_o / 2\pi$ is the resonance frequency of the transducer.

The boundary condition given in Eq. (2) are determined completely by the following two independent dimensionless parameters:

$$A_p = \alpha_o R_o, \quad N_p = \frac{R_o}{z_N} \quad (3)$$

The subscript p, and subsequently f, is used to distinguish between the parameters for plane and focused sources, respectively. Both parameters in Eq. (3) are normalised by the Rayleigh distance $R_o = \omega_o a^2 / 2c_o$. In the definition of the absorption parameter A_p, $\alpha_o = b\omega_o^2 / 2\rho_o c_o^3$ is the thermoviscous attenuation coefficient at frequency ω_o. Thus, A_p is the ratio of the characteristic diffraction and absorption length scales. In the nonlinearity parameter N_p, $z_N = \rho_o c_o^3 / \beta \omega_o p_o$ is the plane wave shock formation distance, an therefore N_p is the ratio of the characteristic diffraction and nonlinearity length scales.

For a focused source with focal length d the boundary condition is given as follows [27, 16]:

$$p(\vec{r}, z=0, t) = p_o \sin\left(\omega_o t + \frac{R_o}{d}\left(\frac{|\vec{r}|}{a}\right)^2\right) H\left(\frac{|\vec{r}|}{a}\right) \quad (4)$$

In that case three dimensionless parameters must be specified:

$$G = \frac{R_o}{d}, \quad A_f = \alpha_o d, \quad N_f = \frac{d}{z_N} \quad (5)$$

where G is the linear focusing gain, equal to the peak value of p/p_o at the geometric focus $(r,z) = (0,d)$ for continuous small-signal radiation at

frequency ω_o in a lossless fluid. The absorption parameter A_f and nonlinearity parameter N_f are scaled here according to the focal length.

3. Measurement set up

Experiments performed in our laboratory allow to obtain some interesting data on properties of finite amplitude sources. Unfortunately the area of observation is limited by dimensions of the tank. Measurements of field distribution of finite amplitude sources are carried out using the experimental arrangement shown in Fig. 1. The examined transmitter and hydrophone are usually positioned along a larger horizontal axis in a tank of water. The tank has dimensions of 1.4 m long by 1.2 m wide and 1.2 m deep. A precise positioning of the transmitter and the receiver during measurements of characteristics of the acoustic sources is very important. A careful alignment of the source and the receiver is particularly indispensable when the pressure distribution at the axis is examined. Therefore high precision equipment has to be used when conducting the above experiments. It consists of three translation guides each perpendicular to each other, all fitted out with stepping motors and controlled automatically. The movement resolution is theoretically equal to 0.0125 mm. The PC used in measurement is also used to control the positioning device.

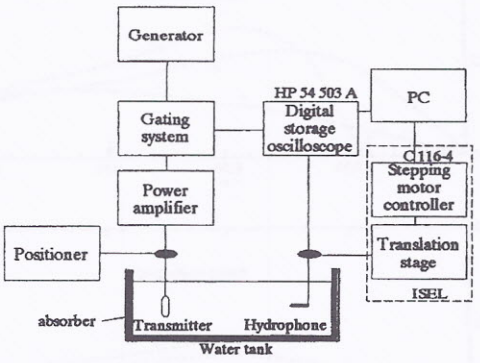

Fig. 1. The measurement set up

For pseudo CW measurements a sinusoidal tone burst of about 50 cycles is applied to the device. The pressure is measured using a needle hydrophone of 1-mm-diam PVdF equipped with preamplifier manufactured by Acoustics Precision Ltd. Its receiving characteristic covers the frequency range from 0.5 MHz up to 20 MHz.

4. Plane circular piston source

The growth of the nonlinear distortion can be noticed by observing the changes in the shape of the wave and in the rising of the amplitude of the higher harmonic components with the increasing distance from the source.

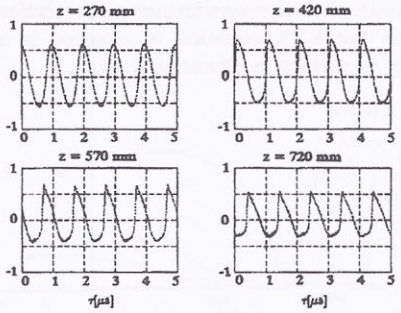

Fig. 2. The changes in the shape of the wave measured on the beam axis with the increasing distance from the source

Fig. 2 shows the shape of the wave measured at different distances from the plane circular piston transmitter of 46-mm-diam and 1.0-MHz center frequency.

Changes in spectrum of the wave during its propagation in nonlinear medium are often used to evaluate the nonlinear distortion. The shape of the wave measured in the axis of the source at the distance of 70 mm, 420 mm and 720 mm, and their respective spectra are presented in Fig. 3.

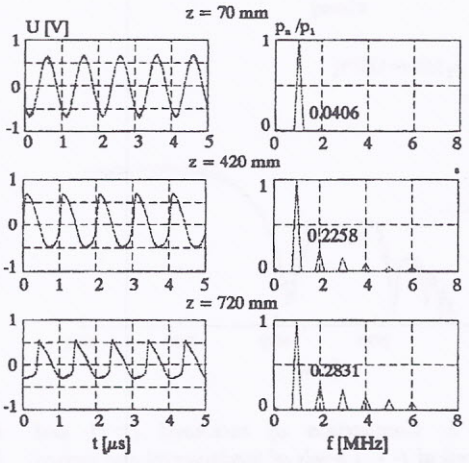

Fig. 3. The shape of the wave measured in the axis of the source at the distance of 70 mm 420 mm and 720 mm and their respective spectra

In the plane distant 720 mm from the source the distortion is quite considerable. The amplitude of the second harmonic equals to about 28% of the amplitude of the first harmonic.

The results of such measurements allow to determine the pattern of pressure distribution. The first comprehensive series of experiments performed for comparison with numerical solution based on the KZK equation is reported in a sequence of articles by Baker et al. [4, 5, 7].

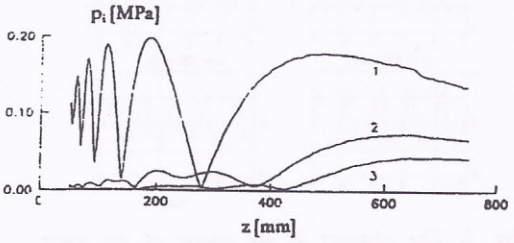

Fig. 4. Measured pressure amplitude of fundamental, second, and third harmonic components along the beam axis of the plane circular source [5]

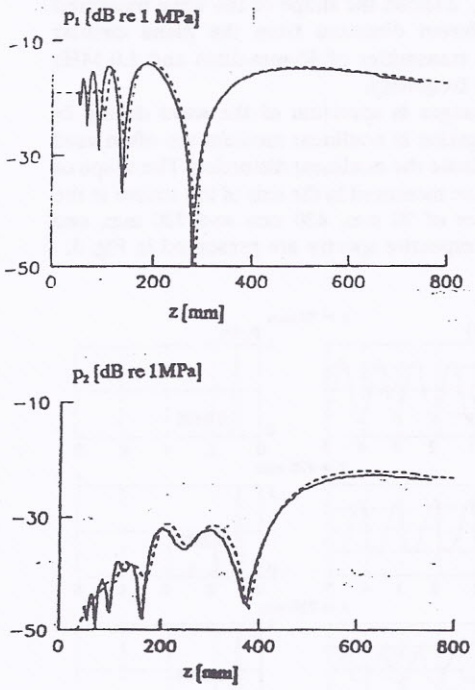

Fig. 5. Comparison of measured (—) and theoretical (- - -) levels of fundamental and second harmonic components along the beam axis [5]

The experimental measurements were made with a plane transducer 38-mm-diam driven at its nominal center frequency of 2.25 MHz corresponding to a *ka* value of 181. The averaged peak pressure across the transducer face was at 100 kPa.

The measured pressure amplitudes along the beam axis for the fundamental, the second and the third harmonic components are shown in Fig. 4, while the comparison between the experimental results and the theoretical prediction is illustrated in Fig. 5. The results of experiment (solid line) are shown together with the results of numerical calculation (dashed line). The comparison could be done from the distance enforced by restriction in validity of the applied numerical model.

The pressure distribution at the radiating surface of real sources not always is uniform. Curves in the next figures (Fig. 6) pointed out the differences in the pressure distribution of the primary wave as well as higher harmonic components.

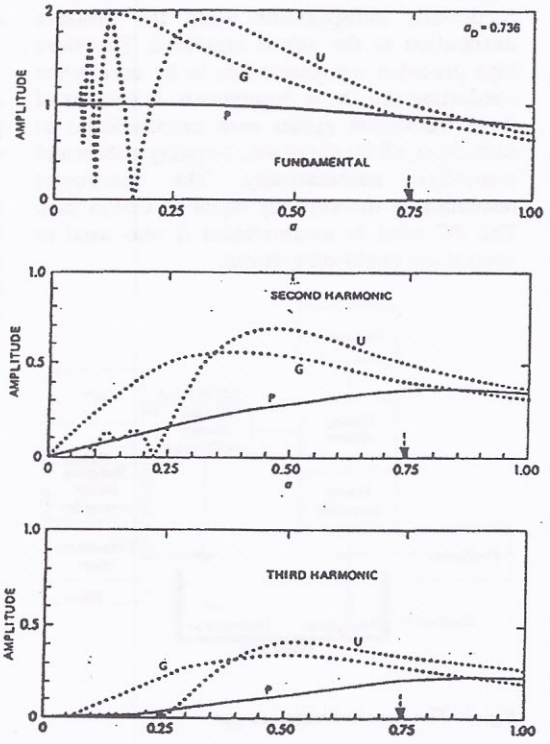

Fig. 6. Pressure distribution of the three first harmonic components versus range computed for various type of sources: U - uniform source, G - Gaussian source, P - plane wave model [1]

Those distributions are obtained theoretically by Aanonsen *et al.* [1] for three various shapes of

pressure distribution at the radiating surface. Apart from that all parameters of the source are assumed to be the same. Calculations are carried out for uniform source (U), for the equivalent Gaussian source (G), and for plane wave model (P). The plane wave shock formation distance in all cases equals to 0.736. The curves approach each other when $\sigma=z/z_N$ is of order one.

Fig. 7 presents the data obtained experimentally for source with nonuniform pressure distribution at the radiating surface. The curve approximating the measured data used in calculation as describing the boundary condition is the one of polynomial type. Results of calculations fit well the ones predicted theoretically and indicate the great impact of the pressure distribution at the source on spatial pattern of the pressure field distribution. The resemblance illustrated in Fig. 7 confirms that it is one of the main factors that influences the phenomena occurring in the vicinity of the source of finite amplitude.

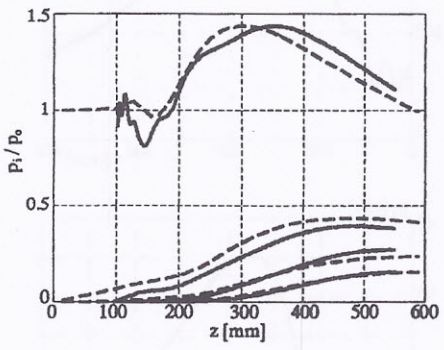

Fig. 7. Pressure distribution of the four first harmonic components along the beam axis obtained assuming polynomial pressure distribution at the source: (- - -), experiment: (——)

5. Focused sources

Features similar to those observed in field of plane sources appear also in focused sound beams. One of the types of examined focused sources is based on a circular plane piston with the additional lens. Baker [4] investigated such focused sources for a wide range of gains. The comparison of measured axial pressure levels with theoretical results for focused sources with gain G=12.09 is shown in Fig. 8, and beam patterns in the focal plane obtained for the source with gain G=3.90 are presented in Fig. 9. The parabolic model used in calculations gives good results on and off the acoustic axis for high levels of nonlinearity. The main difficulty was encountered in determining the precise initial conditions for the model, in particular the focal length and drive level.

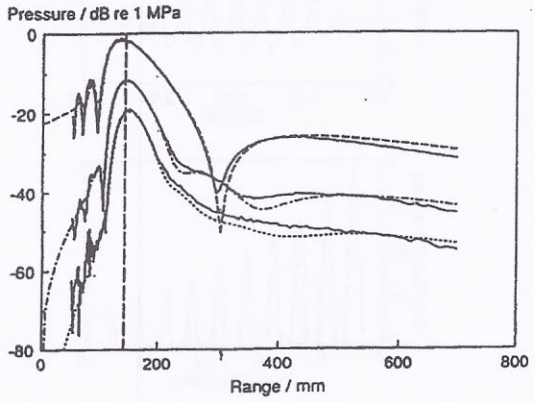

Fig. 8. Comparison of measured pressure levels (——) with theory for fundamental, second and third harmonic components along the axis of the source with additional lens, G=12.09 [4]

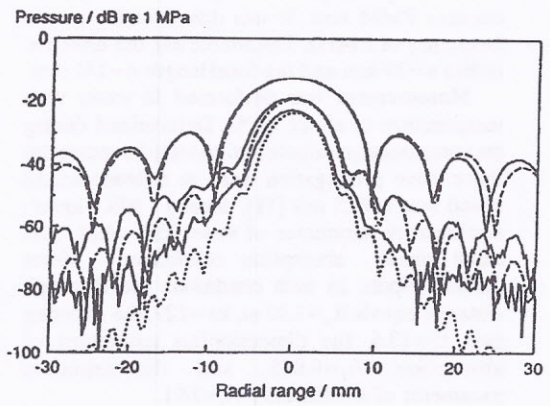

Fig. 9. Beam patterns of fundamental, second and third harmonic components measured in the focal plane (——) with theory (- - -) obtained for the source with additional lens, G=3.90 [4]

The second type of focused sources is based on a single PZT element in a form of focusing bowl. Detailed measurements of such sources were carried out by Averkiou and Hamilton [2], also in a pulse mode [3]. Measurements of the wave-form and corresponding frequency spectrum for shock

formation in a pulse at the geometric focus *(z=d)*, with $d/z_N=0.34$ are illustrated in Fig. 10.

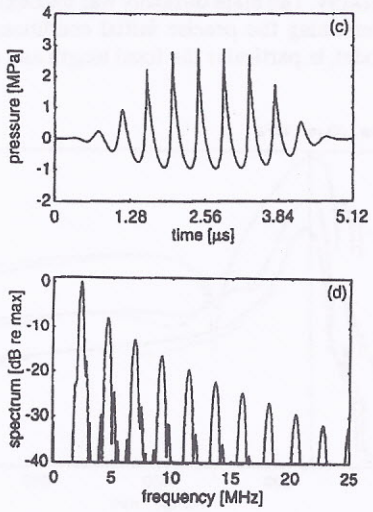

Fig. 10. Wave-form and corresponding spectrum at the geometric focus in the field of a focused circular piston [3]

For our investigations of focused sources we used two types of them. The first one is based on a circular plane piston coupled to the plano-concave PMM lens. It was driven at its central frequency of 1 MHz. The source has the effective radius a=29 mm and the focal length d=141 mm.

Measurement was performed in water with temperature of about 19 °C. Determined during measurements parameters of water influencing the finite wave propagation were as follows: sound speed was 1479.5 m/s [11], density - 998.4 kg/m^3, nonlinearity parameter of water B/A=4.86, and small signal absorption coefficient - about 0.00234 Np/m. In such conditions the Rayleigh distance equals R_o=1.92 m, ka=127, the focusing gain G=13.6, the dimensionless parameter of absorption A_f=0.045, and dimensionless parameter of nonlinearity N_f=1.91.

The changes in the amplitude of the pressure along the axis are shown in Fig. 11. The distribution of the four first harmonic components predicted theoretically illustrates the upper figure, while the results of measurements are shown below it. In the middle picture we can see the pressure distribution of the fundamental component and at the bottom the pressure distribution of higher harmonic components (2-5).

The second of examined sources is based on a single PZT element in a form of focusing bowl. The source is driven at its central frequency 1.5 MHz. It has the effective radius a=25 mm and the focal length d=100 mm.

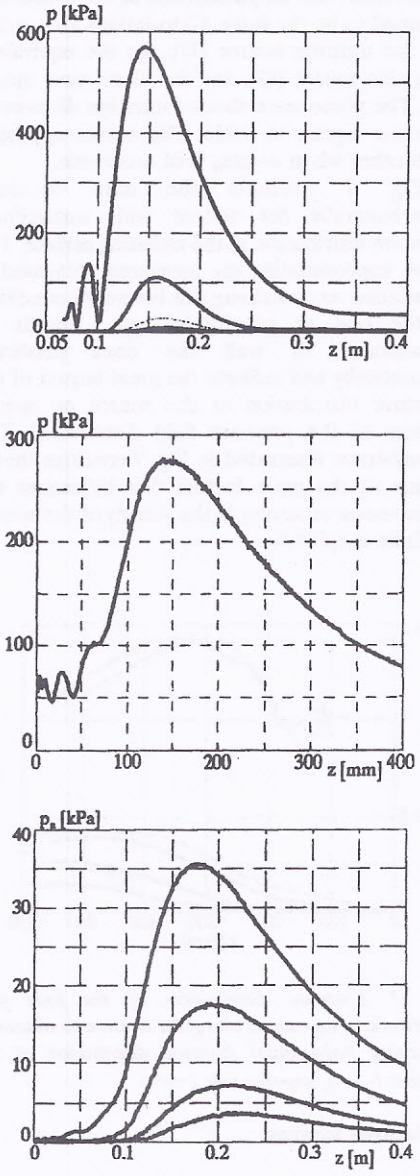

Fig. 11. The distribution of the pressure along the axis of the source with additional lens

Measurement was performed in water with temperature of about 20 °C. Determined during measurements parameters of water influencing the finite wave propagation were as follows: sound speed was of 1484 m/s [11], density - of 998.0 kg/m^3, nonlinearity parameter of water B/A=4.91, and small signal absorption coefficient - about 0.00234 Np/m. In such conditions the Rayleigh

distance equals R_o=1.97 m, ka=158, the focusing gain G=19.7, the dimensionless parameter of absorption A_f=0.1109. The investigations were carried out for radiating pressure of various values, therefore dimensionless parameter of nonlinearity N_f changed from 0.3823 to 3.6663.

Results obtained during measurements of moderate distorted wave are presented in Fig. 12. We can see the first and the second harmonic components distributions along the beam axis. The results of experiment (solid line) are shown together with the results of numerical calculation (dashed line). The comparison could only be done starting from certain distance from the source because of the existing limitations of the applied numerical model.

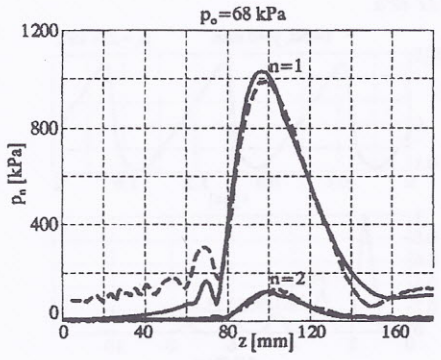

Fig. 12. The pressure distribution of the first and the second harmonic components along the beam axis of the single PZT element focused source

The measured distortion of the wave is lower than the one predicted theoretically for the source with an additional lens. The ratio of the pressure amplitude at the focus to the amplitude at the source's surface as well as the ratio of the maximal pressure amplitudes of higher harmonic components to the amplitude at the source's surface are lower than the theoretical ones. However the area of increased pressure (the focus region) is larger than the expected one. It could be caused by nonuniform pressure distribution on the radiating surface, while in theoretical calculation the pressure distribution was assumed to be uniform. The agreement between results obtained theoretically and experimentally for the single PZT bowl element source is much higher.

The spreading of the sound beam in the post focal region may be assessed using patterns of pressure distribution at planes perpendicular to the beam axis. The transverse pressure distribution of the first harmonic component at the distance of 2d, 3d, 4d and 7d is shown in Fig. 13, whereas the distribution of the three first harmonics at the distance 2d is presented in Fig. 14.

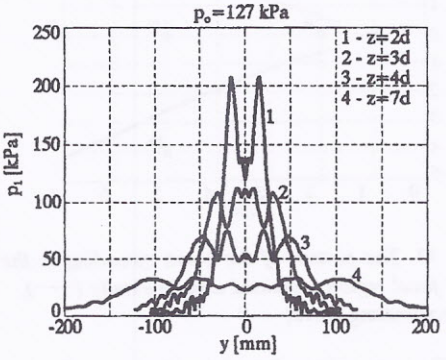

Fig. 13. The transverse pressure distribution of the first harmonic component at the distance of 2d, 3d, 4d and 7d

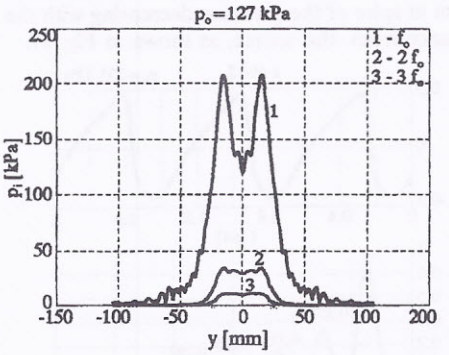

Fig. 14. The pressure distribution of the three first harmonic components at the distance of 2d

Assuming the distance between the maxima of the extremal side-lobes (most distant from the beam axis) to be the width of the beam, the pattern of the beam spreading could be obtained as shown in Fig. 15.

The maxima of the last side-lobes in characteristics of the second harmonic components occur approximately at the same distance as in characteristics of the first ones. The empirically obtained curve bordering the beam could be approximated to the one described as follows:

$$\frac{y}{a} = 0.0248*(\frac{z}{d})^2 + 0.4990*\frac{z}{d} - 0.5029 \qquad (6)$$

where: z/d is the distance expressed in terms of the focal length.

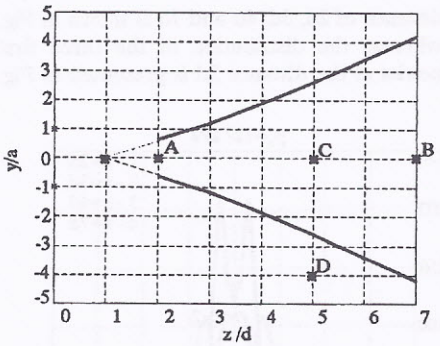

Fig. 15. The pattern of the beam spreading in the post focal region: obtained experimentally (——), approximating curve(- - -)

The examples of registered shape of wave within the beam and its spectrum are presented in Fig. 16. The wave-form remains almost invariable within the bordered area along and crosswise the beam in spite of the pressure decreasing with the distance from the source, as shown in Fig. 17.

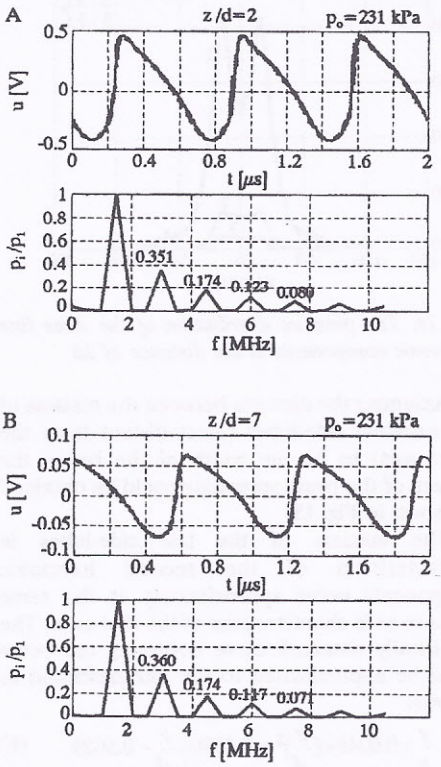

Fig. 16. The shape of wave at the beam axis and its spectrum measured at the distance 2d and 7d from the source

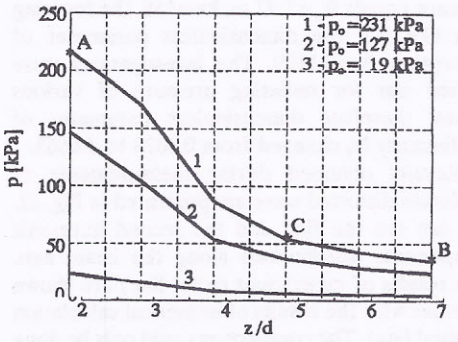

Fig. 17. Changes in pressure along the beam axis in the post focal region for various pressure value at the source: 1 - p_o=231 kPa, 2 - p_o=127 kPa, 3 - p_o=127 kPa

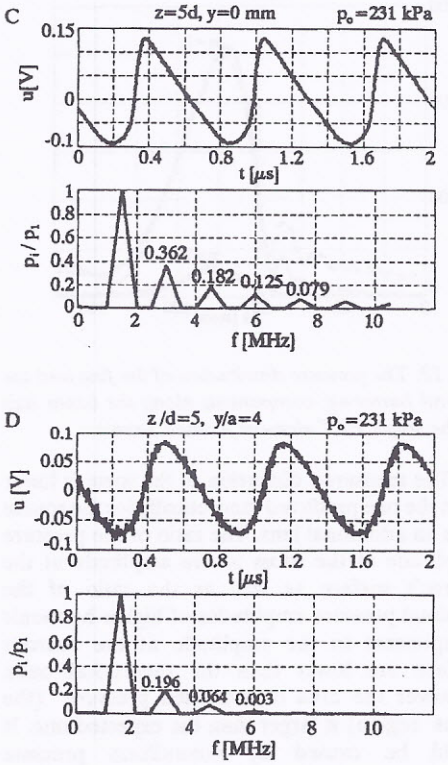

Fig. 18. The shape of wave and its spectrum measured at the beam axis and outside the border of beam at the plane distant of 5d from the source

Obtained results confirm slight changes in spectrum of the wave within the beam. For instance, in the case when pressure at the source p_o=231 kPa, the differences in spectra determined on the axis at the distance 2d and 7d are

following: the second harmonic component normalised to the first increases by about 2.5%, the third remains nearly the same, the fourth decreases by 4.8% and the fifth decreases by 10.7%. The differences in spectra determined at the same distance (5d) on axis and at the border of the beam are greater. The second harmonic components decrease by about 23% , the third - by 30%, the fourth - by 41% and the fifth - by 52%. Outside the border of beam the nonlinear distortion fades out more rapidly than inside as pointed in Fig. 18.

The presented results of investigation of focused field in the post focal region lead to the conclusion that in that area up to certain distance wave propagates as a wave of steady shape. It propagates as a beam with border determined by the maxima of the extremal side-lobes in the transverse pressure distribution. The change in spectrum across the axis is faster than along the axis, where it is very slow. The spreading of the beam could be treated roughly as linear in the considered area.

6. Conclusions

The paper presents the results of the experimental investigations of the finite amplitude wave field distribution. The measurement results obtained using the high precision facility which controlled the movement of the receiver. It contains also the results of measurements together with calculations allow to make a thorough study of the nonlinear distortion growth in the pressure field of finite amplitude sources. They confirm the usefulness of both the elaborated method and the measurement set up for the investigations, especially in the vicinty of the source.

The presented results of measurements provide valuable information on pressure field of examined sources. The investigations of such a kind, in spite of the fact that they are highly time-consuming, are particularly useful in the case of sources with complex radiating surface for which theoretical evaluation may prove to be extremely complicated or even impossible.

7. Acknowledgments

The research was supported by the State Committee of Scientific Research grant No 7 T07B 072 14.

Reference

1. I. Aanonsen, T. Barkve, J. Naze Tjøtta, S. Tjøtta, Distortion and harmonic generation in the nearfield of a finite amplitude sound beam, J. Acoust. Soc. Am., 75, pp. 749-768, (1984).

2. M. A. Averkiou and M. F. Hamilton, Measurements of harmonic generation in a focused finite-amplitude sound beam, J. Acoust. Soc. Am., 98, pp. 3439-3442, (1995).

3. M. A. Averkiou and M. F. Hamilton, Nonlinear distortion of short pulses radiated by plane and focused circular pistons, J. Acoust. Soc. Am., 102, pp. 2539-2548, (1997).

4. A. C. Baker, Nonlinear pressure fields due to focused circular apertures, J. Acoust. Soc. Am., 91, pp. 713-717, (1992).

5. A. C. Baker, K. Anastasiadis, V. F. Humprey, The nonlinear pressure field of a plane circular piston: Theory and experiment, J. Acoust. Soc. Am., 84, pp. 1483-1487, (1988).

6. A. C. Baker, A. M. Berg, A. Sahin, J. Naze Tjøtta, The nonlinear pressure field of a plane, rectangular apertures: Experimental and theoretical results, J. Acoust. Soc. Am., 97, pp. 3510-3517, (1995).

7. A. C. Baker, V. F. Humprey, Distortion and high-frequency generation due to nonlinear propagation of short ultrasonic pulses from a plane circular piston, J. Acoust. Soc. Am., 92, pp. 1699-1705, (1992).

8. N. S. Bakhvalov, Ya. M. Zhileikin, E. A. Zabolotskaya, *Nonlinear Theory of Sound Beams,* Moscow: Nauka, 1982.

9. D. Cathignol, J. Y. Chapelon, High energy ultrasound therapy, Part I and Part II, Advances in nonlinear acoustics, World Scientific, London, pp. 21-35, (1993).

10. J. Dybedal, TOPAS: Parametric end-fire array used in offshore applications, Advances in nonlinear acoustics, World Scientific, London, pp. 264-269, (1993).

11. H. Endo, Calculation of nonlinearity parameter for seawater, J. Acoust. Soc. Am., 76, pp. 274-277, (1984).

12. L. Filipczyński, J. Etienne, M. Piechocki, An attempt to reconstruct the lithotripter shock wave pulse in kidney: Possible temperature effects, Med. Biol., 18, pp. 569-577, (1992).

13. L. Filipczyński, T. Kujawska, R. Tymkiewicz, J. Wójcik, Nonlinear and linear propagation of diagnostic ultrasound pulses, Ultrasound in Med. and Biol., 25, pp. 285-299, (1999).

14. L. Germain, J. D. N. Cheeke, Generation and detection of high order harmonics in liquids using a scanning acoustic microscopy, J. Acoust. Soc. Am., 83, pp. 942-949, (1988).

15. X. F. Gong, X. Z. Liu, Acoustical nonlinearity parameter and its medical applications, Advances in nonlinear acoustics, World Scientific, London, pp. 353-357, (1993).

16. H. Hobaek and B. Ystad, Experimental and numerical investigation of shock wave propagation in the post focal region of a focused sound field, ACUSTICA - Acta Acustica, 83, pp. 978-986, (1997).
17. F. Ingenito, A. O. Williams Jr., Calculation of second harmonic generation in a piston beam, J. Acoust. Soc. Am., 49, pp. 319-328, (1971).
18. E. Kozaczka, G. Grelowska, Nonlinearity parameter B/A of the low-salinity seawater, Arch. Acoust., 19, pp. 259-270, (1994).
19. Y. S. Lee, M. F. Hamilton, Time-domain modeling of pulsed finite amplitude sound beams, J. Acoust. Soc. Am., 97, pp. 906-917, (1995).
20. S.-W. Li, Z.-X. Xu, The harmonic nearfield of a narrow strip transducer, Nonlinear acoustics in perspective, Nanjing University Press, pp. 200-205, (1996).
21. B. G. Lucas and T. G. Muir, The field of a focusing source, J. Acoust. Soc. Am., 72, pp. 1289-1296, (1982).
22. B. G. Lucas and T. G. Muir, Field of a finite-amplitude focusing source, J. Acoust. Soc. Am. 74, pp. 1522-1528, (1983).
23. B. E. McDonald, W. A. Kuperman, Time domain formulation for pulse propagation including nonlinear behaviour at a caustic, J. acoust. Soc. Am., 81, pp. 1406-1417, (1985).
24. J. A. TenCate, An experimental investigation of the nonlinear pressure field produced by a plane circular piston, J. Acoust. Soc. Am., 94, pp. 1084-1089, (1993).
25. J. N. Tjotta, S. Tjotta, Nonlinear equations of acoustics, with application to parametric acoustic arrays, J. Acoust. Soc. Am., 69, pp. 1644-1652, (1981).
26. J. N. Tjøtta, S. Tjøtta, E. H. Vefring, Propagation and interaction of two collimated finite amplitude sound beams, J. Acoust. Soc. Am. 88, pp. 2859-2870 (1990).
27. E. H. Vefring, J. N. Tjotta, S. Tjotta, Effects of focusing on the nonlinear interaction between two collinear finite amplitude sound beams, J. Acoust. Soc. Am., 89, pp. 1017-1027, (1991).